Pulsed-field magnetization, electron spin resonance, and nuclear spin-lattice relaxation in the $\{Cu_3\}$ spin triangle

Kwang-Yong Choi and Naresh S. Dalal
Department of Chemistry and Biochemistry, Florida State University and National High Magnetic Field Laboratory, Tallahassee, Florida 32306-4390, USA

Arneil P. Reyes and Philip L. Kuhns
National High Magnetic Field Laboratory, Tallahassee, Florida 32310, USA

Yasuhiro H. Matsuda and Hiroyuki Nojiri
Institute for Materials Research, Tohoku University, Katahira 2-1-1, Sendai 980-8577, Japan

Sib Sankar Mal and Ulrich Kortz
School of Engineering and Science, Jacobs University Bremen, P.O. Box 750 561, 28725 Bremen, Germany
(Received 20 August 2007; published 8 January 2008)

We report on pulsed-field magnetization, Q-band electron spin resonance (ESR), and ^{23}Na NMR measurements of the $S=1/2$ spin triangle clusters $Na_9[Cu_3Na_3(H_2O)_9(\alpha\text{-}XW_9O_{33})_2]$ (X=As and Sb). The pulsed-field magnetization shows pronounced hysteresis loops and magnetization steps including the half-step magnetization. The detailed magnetization behavior depends substantially on the diamagnetic heteroatom X. The angular dependence of ESR parameters necessitates Dzyaloshinskii-Moriya interaction. The temperature dependence of the ^{23}Na spin-lattice relaxation rate, $1/T_1$, scales well to $\chi(T)T$, where $\chi(T)$ is the static susceptibility. The spin-spin relaxation rate, $1/T_2$, increases rapidly for temperatures below 15 K due to dipolar interactions between the ^{23}Na nuclei and Cu^{2+} spins. The two clusters exhibit a markedly different field dependence of $1/T_1$ at antilevel crossing points. The enhancement of $1/T_1$ is noticeable only for X=Sb. Since the spin configurations of both clusters are nearly the same, the dependence of magnetization and $1/T_1$ on X is ascribed to the strong coupling of the spins to a lattice vibration, leading to an enhanced mixing of the $S=1/2$ chiral state.

DOI: 10.1103/PhysRevB.77.024406 PACS number(s): 75.50.Xx, 75.45.+j, 33.25.+k, 33.35.+r

I. INTRODUCTION

In recent years, magnetic molecules consisting of a small number of exchange-coupled paramagnetic ions have been intensively investigated.[1,2] This is due to the fact that they offer an opportunity for exploring the basic principles of nanomagnets and have the technological potential for miniaturization of electronic devices to molecular scale.

Two different classes of magnetic molecules have, in particular, acquired strong research interest. One class is the single molecule magnets (SMMs), which behave like a single magnet with magnetic anisotropy. Their prominent features are a magnetic bistability, quantum tunneling of magnetization, and quantum phase interference (Berry phase).[3–5] The other one is antiferromagnetically coupled spin rings. Their fundamental aspect is that the elementary excitations are described by a quantized rotation of the Néel vector.[6] In the antiferromagnetic (AF) spin rings, the tunneling gap can be as large as several percent of the isotropic exchange coupling constants. In contrast, the gap from SMMs is usually limited to the millikelvin range. Thus, the AF spin rings have the advantage of revealing pure quantum magnetization over the SMMs because the large tunneling gap strongly suppresses thermal effects.

Among the AF spin rings, triangular rings are the simplest system. Moreover, they hold a special position in the magnetism due to the effects of spin frustration and spin chirality.[7–11] A prototypical example is found in the $\{V_6\}$-, $\{V_{15}\}$-, $\{Cu_3\}$-, and $\{Mn_3O\}$-type triangular antiferromagnets.[10–14] In the $\{Cu_3\}$ spin triangle, a half-step magnetization appears as adiabatic quantum tunneling. Very recently, isosceles AF spin rings have been proposed for a basic unit of molecule-based quantum computation.[15] For a realistic implementation of quantum-information processing, all sources of decoherence are needed to be clarified. Nuclear spins and intermolecular dipolar interactions are mostly the well-known ones.[16] In addition, spins can undergo a decoherence through coupling to lattice vibrations.[17] This might be related to distinct material dependence of the magnetization in the $\{V_3\}$ spin triangle.[8] However, the exact mechanism still remains unclear. In this work, we address this issue by studying two $\{Cu_3\}$ spin triangles having slightly different molecular environments.

The copper(II)-substituted polyoxotungstates $Na_9[Cu_3Na_3(H_2O)_9(\alpha\text{-}XW_9O_{33})_2]$ (abbreviated as $\{Cu_3\text{-}X\}$ with X=As and Sb) have a sandwich-type structure with D_{3h} symmetry, where $\{Cu_3\}$ resides in the central belt and is capped by two $(\alpha\text{-}XW_9O_{33})$ Keggin subunits [see Fig. 1(a)].[18,19] Spin exchange couplings between Cu^{2+} ions occur in an indirect way via two W and three O atoms of each (XW_9O_{33}) fragment. This enables us to modify the magnitude of spin interactions by replacing the diamagnetic heteroatom X. Figures 1(b) and 1(c) depict the spin topology of $\{Cu_3\text{-}X\}$. For $\{Cu_3\text{-As}\}$, the distances between the copper ions are $Cu_1\cdots Cu_2$=4.696 Å and $Cu_2\cdots Cu_2$=4.689 Å, while for $\{Cu_3\text{-Sb}\}$, the respective distances increase slightly to

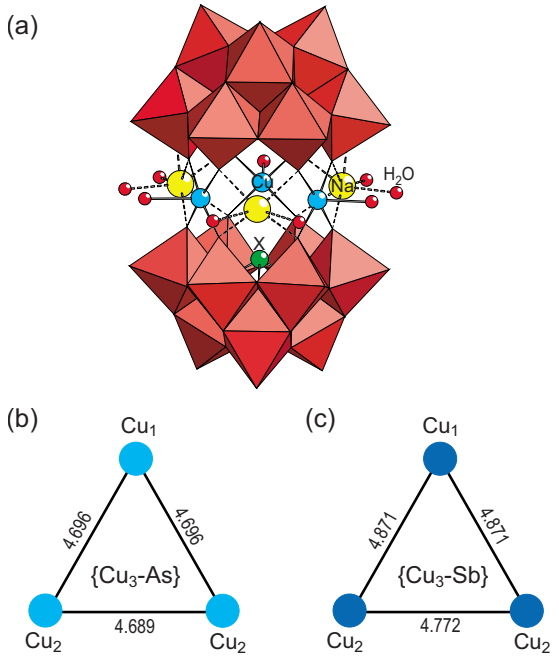

FIG. 1. (Color online) (a) Combined polyhedral/ball-and-stick representation of $Na_9[Cu_3Na_3(H_2O)_9(\alpha\text{-}XW_9O_{33})_2]$. Yellow ball is for Na atoms, cyan for Cu, green for X, and red for H_2O. [(b) and (c)] Sketch of the {Cu_3-X} spin triangle configuration with Cu···Cu distances. Cu_1 and Cu_2 represent two crystallographically inequivalent Cu sites. The numbers on the solid lines are Cu···Cu distances.

$Cu_1\cdots Cu_2$=4.871 Å and $Cu_2\cdots Cu_2$=4.772 Å. This is thought to be caused by the difference of lone pair–lone pair interactions between the two X atoms. Since Sb has a larger atom size than As, the lone pair interactions between Sb become stronger, leading to a larger separation of the copper centers.

In what follows, we report pulsed-field magnetization, Q-band electron spin resonance (ESR), and ^{23}Na NMR spin-lattice relaxation time (T_1) measurements on the {Cu_3-X} family. We find that the detailed features of the magnetization and nuclear spin-lattice relaxation rate depend on the diamagnetic heteroatom X although their electronic magnetic parameters are only marginally different. This suggests that there is a strong coupling between the spin and the lattice vibrations which causes X-dependent enhanced T_1 relaxation at electron spin energy level crossings.

This paper is organized as follows. In Sec. II, we describe the experimental setup and conditions. In Sec. III, we present the experimental results of magnetization and electron and nuclear spin resonances. The discussion of the respective experimental results is given in Sec. IV. Section V provides a summary of our findings.

II. EXPERIMENTAL DETAILS

Single crystals of $Na_9[Cu_3Na_3(H_2O)_9(\alpha\text{-}AsW_9O_{33})_2]\cdot 26H_2O$ and $Na_9[Cu_3Na_3(H_2O)_9(\alpha\text{-}SbW_9O_{33})_2]\cdot 40H_2O$, respectively, were prepared as described in Ref. 18. For pulsed magnetization experiments, a dozen of small single crystals were glued together along the field $H\|$ triangle plane. Magnetization measurements were carried out by means of a standard inductive method using compensated pickup coils and a nondestructive pulse magnet. Fast pulsed magnetic fields up to 10^3 T/s were generated by a capacitor bank of 90 kJ as described in Ref. 20. The sample was immersed in liquid ^{3}He to reach a temperature as low as 0.4 K. ESR measurements of a single crystal were performed using a commercial Bruker spectrometer operating at the Q band ($\nu\approx 34$ GHz). ^{23}Na NMR spectrum of powder samples was obtained using a locally developed NMR spectrometer and a high homogeneity 15 T sweepable magnet.[21]

III. EXPERIMENTAL RESULTS

A. Pulsed-field magnetization

Shown in Fig. 2 is the magnetization versus magnetic field plot for {Cu_3-X} at 0.4 K for H oriented in the plane comprising the spin triangle. The measurements were performed in a full cycle sweep at a time scale of about 5 milliseconds. A time evolution of a pulsed field is plotted in the inset of Fig. 2. We note that the saturation magnetization is renormalized by gS. Here, the g-factor is determined by electron spin resonance as discussed below.

In the upward sweep ($A\rightarrow B$), the magnetization of {Cu_3-As} first increases to $1gS\mu_B$, followed by the step of $2.3gS\mu_B$, and finally approaches the saturation value of $3gS\mu_B$ in a high magnetic field of 12 T. In the down sweep ($B\rightarrow C$), the magnetization drops sharply from $3gS\mu_B$ to $1gS\mu_B$ and from $1gS\mu_B$ to zero, respectively. The former $2gS\mu_B$ step originates from the level crossing between $S^T=1/2$ and $S^T=3/2$ states. The latter $1gS\mu_B$ one is related to a splitting of the $S^T=1/2$ state at zero field (see below for more details). The $1.3gS\mu_B$ step seen in the upward sweep cannot be understood within a simple energy level scheme of a spin triangle. The contrasting magnetization between the up and down sweeps leads to a pronounced hysteresis loop. In the negative field, the hysteresis behavior nearly disappears. The magnetization of the negative field is similar to the magnetization which is seen in the down sweep of the positive field. We stress that the hysteresis loop is not associated with an energy barrier since Cu^{2+} has no single ion anisotropy and the Cu^{2+} triangle is coupled antiferromagnetically. Rather, the asymmetric magnetization through the positive and negative fields implies that the magnetization reversal dynamics is slow on the time scale of the pulsed-field sweep rate.

Upon switching to {Cu_3-Sb}, the magnetization steps become less sharp in comparison to {Cu_3-As}. In addition, the magnetization curve looks more symmetric between the positive and negative fields. This is mainly due to the smearing of the $2.3gS\mu_B$ step in the positive field and the appearance of the small step in the negative field between −5 and −7 T, which is absent in {Cu_3-As}. The dependence of the magnetization on the heteroatom X suggests that the dynamical magnetization processes are distinctly different in the two compounds.

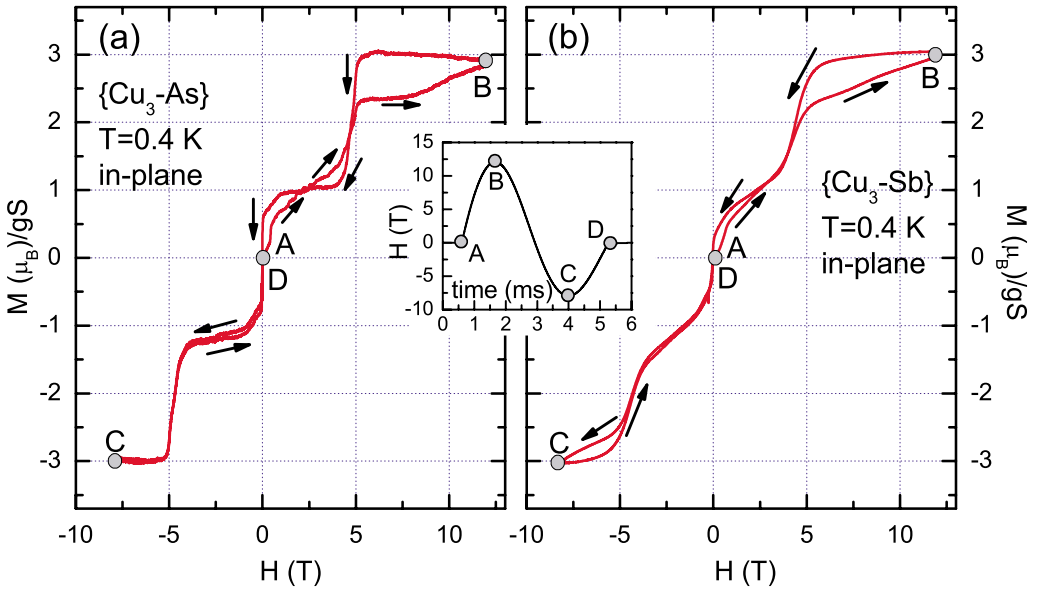

FIG. 2. (Color online) (a) Magnetization curve vs pulsed magnetic field for $\{Cu_3\text{-As}\}$ at 0.4 K for $H\|$ triangle plane. The saturated magnetization is normalized by gS. Arrows are a guide to sweep directions ($A\rightarrow B\rightarrow C\rightarrow D$). (b) Magnetization of $\{Cu_3\text{-Sb}\}$ using a pulsed field with the same conditions as (a). The inset shows the time dependence of a pulsed magnetic field.

B. Electron spin resonance

ESR spectra of $\{Cu_3\text{-As}\}$ recorded at 8.8 K and $\nu=34$ GHz are presented in Fig. 3 as a function of angle. The angle is measured between the molecular C_3 axis and the external field. The three intense peaks ranging from 1.1 to 1.2 T correspond to the electron spin transitions between the excited $S^T=3/2$ levels. The respective transitions are assigned according to the calculated level diagram (refer to Fig. 8 for the numeric designations of the energy levels). In addition, we also observe several weak transitions arising from the $S^T=1/2$ levels. We note that the ESR intensity of the $S^T=1/2$ group is much weaker than that of the $S^T=3/2$ group although the ESR signals of the $S^T=3/2$ group are from the excited states. The weaker intensity of the $S^T=1/2$ group is due to the reduced magnitude of the spin number S since the ESR transition probability is given by $P\propto[S(S+1)-S_z(S_z+1)]$.

The ESR signals of the $S^T=1/2$ group consist of the conventional ($\Delta M_z=\pm1$) ESR transitions of $|1\rangle\rightarrow|3\rangle$ and $|2\rangle\rightarrow|4\rangle$ as well as of the symmetry-forbidden transitions of $|1\rangle\rightarrow|4\rangle$. The forbidden transitions show the opposite angular dependence to the allowed ones [compare Figs. 4(b) and 4(c)]. In addition, they show a strong angular dependence in intensity (see the left panel of Fig. 3). The signals are hardly observable when the sample is rotated such that the external field is along the triangle plane. The presence of the symmetry-forbidden signals implies nonvanishing matrix elements between the energy levels 1 and 4. This highlights the significant role of Dzyaloshinskii-Moriya (DM) interactions in understanding the magnetic behavior of $\{Cu_3\text{-}X\}$. Here, we note that the matrix elements can vary strongly with magnetic field orientation since a mixing between the energy levels is determined by the sign and magnitude of DM interactions.

Figure 4(a) displays the temperature dependence of the ESR intensities of the $|7\rangle\rightarrow|8\rangle$ (full triangle) and $|6\rangle\rightarrow|7\rangle$ (open rectangle) transitions. They scale roughly with the magnetic susceptibility $\chi(T)$. The g-factors of the respective transitions are plotted as a function of temperature in the

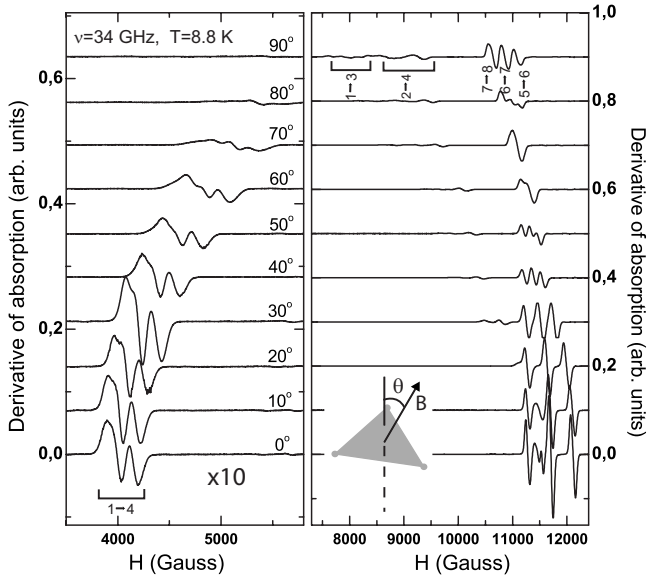

FIG. 3. Angular dependence of ESR spectra (derivative of the absorption spectra versus field, vertically shifted for clarity) measured at $\nu=34$ GHz and 8.8 K for $\{Cu_3\text{-As}\}$. The angle is measured between the C_3 axis of a triangle and the external field. The three strong peaks of the right panel correspond to the transitions between the $S^T=3/2$ states. The weak peaks arise from the transitions between the $S^T=1/2$ states. Note the different magnetic field scales of the left and right panels, and ESR spectra of the left panel are ten times magnified.

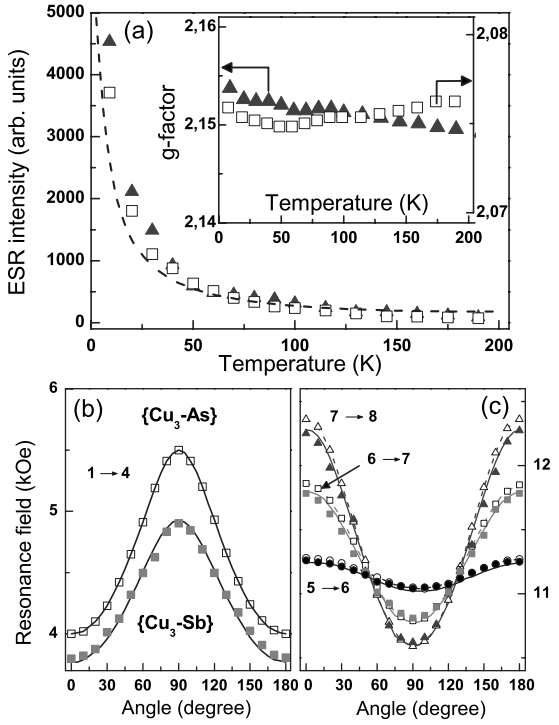

FIG. 4. (a) Temperature dependence of ESR intensity of the $|7\rangle \rightarrow |8\rangle$ (full triangle) and $|6\rangle \rightarrow |7\rangle$ (open rectangle) transitions. The inset displays the respective g-factor as a function of temperature. [(b) and (c)] Angular dependence of the resonance fields. The open (full) symbols represent the experimental data of $\{Cu_3\text{-As}\}$ ($\{Cu_3\text{-Sb}\}$).

inset of Fig. 4(a). No appreciable change is detected. This rules out any significant structural modulations with temperature change.

Figures 4(b) and 4(c) summarize the angular dependence of the resonance fields. The open (full) symbols represent the experimental data of $\{Cu_3\text{-As}\}$ ($\{Cu_3\text{-Sb}\}$). Overall, the resonance fields of $\{Cu_3\text{-Sb}\}$ are lower than those of $\{Cu_3\text{-As}\}$. This suggests that the magnetic parameters of $\{Cu_3\text{-}X\}$ are reduced upon replacing As with Sb. This is consistent with the increasing distances between the copper ions in $\{Cu_3\text{-Sb}\}$.

C. Nuclear spin resonance

To investigate the dynamics of the Cu^{2+} electronic spins, we have performed NMR measurements using the ^{23}Na nuclei which are coupled via dipole-dipole interactions to the Cu^{2+} magnetic moments. Since three Na^+ nuclei are located between the Cu^{2+} spins [see Fig. 1(a)], they discriminate the spin dynamics of each Cu^{2+} ion. In contrast, we note that the ^1H nuclei do not provide specific information since the H atoms have spatially two different classes. The H_2O molecules inside the central belt of the cluster are directly coupled to the Cu spins, while other ^1H nuclei lie far away [see Fig. 1(a)]. Thus, we will focus on the ^{23}Na NMR measurements in this study.

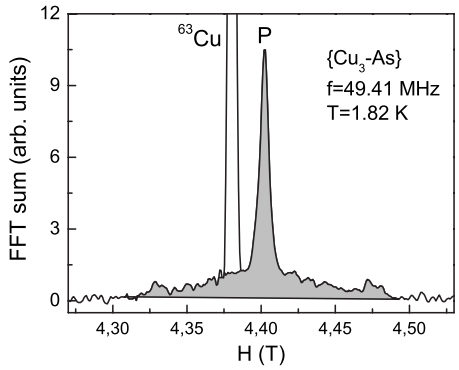

FIG. 5. ^{23}Na NMR spectrum obtained by monitoring the FFT sum of a spin echo as a function of an external field at a fixed temperature of 1.82 K. The shaded area indicates the ^{23}Na NMR spectrum, which consists of the $+1/2 \leftrightarrow -1/2$ central transition (marked P) and the quadrupolar wings. The empty solid line is ^{63}Cu NMR spectrum from the rf coil. The T_1 measurements were made on the peak P.

A typical ^{23}Na NMR spectrum is displayed in Fig. 5. The spectrum was obtained by monitoring the fast Fourier transform (FFT) sum of a spin echo as a function of an external field at a fixed temperature of 1.82 K. We observe a peak, labeled P, together with its quadrupolar wings. The ratio between the intensity of the peak P and the wings is 0.57, close to the theoretical value of 2/3. This confirms that the peak P originates from the $+1/2 \leftrightarrow -1/2$ central transition. We note that the sharp, intense peak next to the peak P is from the copper coil and not from the sample since the magnetic moment sits on the Cu^{2+} ion.

We measured the ^{23}Na nuclear spin-lattice relaxation rate $1/T_1$ in the temperature range between 1.8 and 50 K at the two fixed magnetic fields $H=2$ and 4.4 T. The peak P was selectively irradiated. The recovery curve of the longitudinal magnetization is fitted by a double exponential function,

$$M(t) = M_\infty[1 - (0.4e^{-t/T_1} + 0.6e^{-t/6T_1})], \qquad (1)$$

characteristic for the central transition of $I=3/2$ nuclei.

Figure 6(a) shows the temperature dependence of $1/T_1$ for $\{Cu_3\text{-As}\}$. For temperature above 50 K, the NMR signal becomes too weak for $1/T_1$ measurements. $1/T_1$ slowly decreases with decreasing temperatures from 50 K and then shows a strong drop below 10 K. This is due to the depopulation of the excited states into the ground state in accordance with the fact that the magnetic properties at low temperatures are governed by the low-lying energy states.

We recall that for even AF rings there exists a strong enhancement of $1/T_1$, leading to a peak at a temperature of the order of the exchange coupling constant J/k_B.[22] In the case of the $\{V_6\}$ AF spin triangle, the temperature dependence of $1/T_1$ is well approximated by $T\chi(T)$ without showing a peak. In contrast, for $\{V_{15}\}$ the enhanced peak of $1/T_1$ occurs around 50–100 K and is attributed to the interlayer exchange couplings.[23,24] In our cluster, the temperature dependence is proportional to $T\chi(T)$ as is the case for $\{V_6\}$. This confirms that the ^{23}Na nucleus probes the spin dynamics

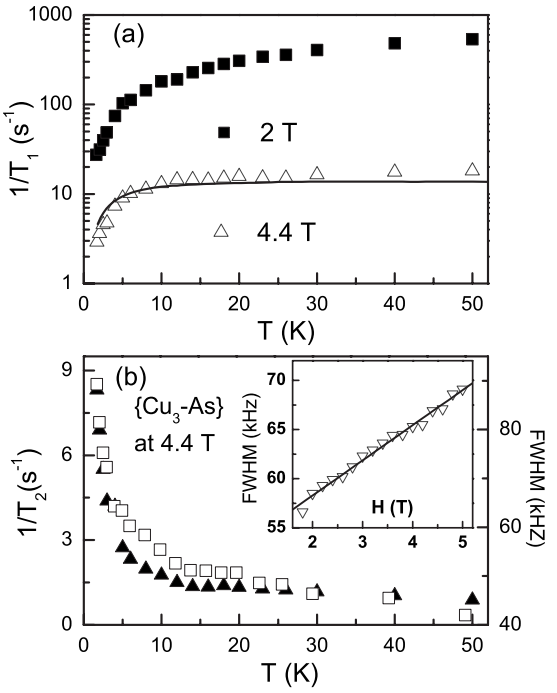

FIG. 6. (a) ^{23}Na spin-lattice relaxation rate $(1/T_1)$ of $\{Cu_3\text{-As}\}$ at 2 T (full square) and 4.4 T (open triangle) as a function of temperature. The solid line is the temperature dependence of $\chi(T)T$ at 4.4 T. (b) Temperature dependence of spin-spin relaxation rate, $1/T_2$, (full triangle) and ^{23}Na FWHM (open square) for $\{Cu_3\text{-As}\}$ at 4.4 T.

of the Cu^{2+} ions, which behave like a paramagnetic ion.

In Fig. 6(b), we show the temperature dependence of the spin-spin relaxation rate $1/T_2$ together with the ^{23}Na linewidth. The recovery of the transverse magnetization is well described by an exponential decay with time. Both $1/T_2$ and the full width at half maximum (FWHM) are more or less constant in the temperature range of 15–50 K. T_2 is of order 1 s in this temperature interval and starts to decrease steeply for temperatures below 15 K. The temperature dependence of $1/T_2$ at low temperatures is opposite to that of $1/T_1$. Since $1/T_1$ scales as $T\chi(T)$, it should not be ascribed to the slowing down of the Cu^{2+} spins. Instead, the low-temperature enhancement of $1/T_2$ could be due to the slowing down of the nuclear relaxation of H and/or Cu nuclei, which are coupled to ^{23}Na nuclei via nuclear dipolar interactions. The inset shows the field dependence of the FWHM versus the external field at 1.7 K. Since the linewidth increases with increasing field, the broadening is not associated with the second-order quadrupole effect on the central transition. Rather, it originates from magnetic dipolar interactions which couple ^{23}Na nuclei to the Cu^{2+} spins. The data are fitted by $\Delta\nu = \alpha H + \Delta\nu_0$.[23] We obtain a local hyperfine coupling factor of $\alpha = 3.6$ kHz T^{-1} and the zero-field value of dipolar interactions of $\Delta\nu_0 = 51.1$ kHz, which seems reasonable.

We now turn to the field dependence of $1/T_1$. The results of $\{Cu_3\text{-}X\}$ are shown in Fig. 7. Both compounds exhibit a strong field dependence on $1/T_1$ as found in other molecular magnets. This is due to the slow decay of the Cu^{2+} ion spin correlation function, which is a characteristic feature of the

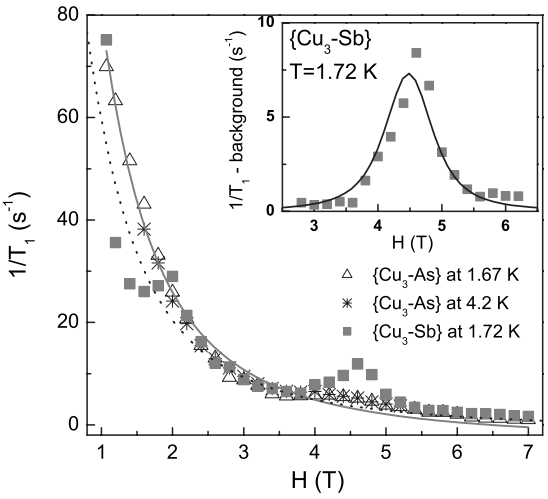

FIG. 7. Field dependence of spin-lattice relaxation rate $1/T_1$ at 1.67 K for $\{Cu_3\text{-As}\}$ compound and at 1.72 K for $\{Cu_3\text{-Sb}\}$ compound, respectively. The solid line is a fit of the data to Eq. (2). Inset: Field dependence of $1/T_1$ subtracted by the background, which is obtained by Eq. (3). The solid line is a calculated curve with $\Delta = 0.6$ K.

zero dimensionality of the system.[10] As in Ref. 10, we analyze the data in terms of the simplified expression

$$T_1^{-1}(T,H) = F_{zz}(T)[1/\omega_0 + \alpha\omega_0/(\omega_e^2 + \omega_0^2)], \qquad (2)$$

where $F_{zz}(T)$ is a sum of the autocorrelation and nearest-neighbor correlation function, ω_0 is an angular frequency measuring the Lorentz broadening, α is given by the ratio between components of the magnetic dipolar interaction tensor, and $\omega_e = \gamma_e H$ is the electronic Larmor frequency. Since the critical enhancement is absent for the studied compounds, ω_0 is weakly T dependent. This is evidenced by the fact that for $\{Cu_3\text{-As}\}$, $T_1^{-1}(H, 4.2\text{ K})$ is well rescaled to $T_1^{-1}(H, 1.67\text{ K})$. A comparison of the fit to the data reveals that $\{Cu_3\text{-Sb}\}$ shows an enhancement of $T_1^{-1}(H,T)$ at the magnetic fields of 2 and 4.5 T, where the antilevel crossings occur between $S^T = 1/2$ and $S^T = 3/2$ (see Fig. 8). Noticeably, it is present but less evident in the $\{Cu_3\text{-As}\}$ compound.

The enhancement of $1/T_1$ at level crossings can be understood in terms of a phenomenological model,[25]

$$1/T_1 = A\Gamma/(\Gamma^2 + [h\omega_L - \Delta(H)]^2), \qquad (3)$$

where A is an average hyperfine coupling constant, Γ is a T-dependent damping factor, and $\Delta(H)$ is the field-dependent energy difference between energy levels. In proximity to the level crossing field, $\Delta(H)$ is written by

$$\Gamma(H) = \{[g\mu_B(H_c - H)]^2 + \Delta^2\}^{1/2},$$

where H_c is a critical field and Δ is an energy gap at level crossing fields. For the analysis of $\{Cu_3\text{-Sb}\}$, we first subtract from the raw data the background calculated by Eq. (2). The subtracted result is shown in the inset of Fig. 7. A reasonable fit is obtained using $H_c = 4.47$ T and $\Delta = 0.6$ K, which are discussed below.

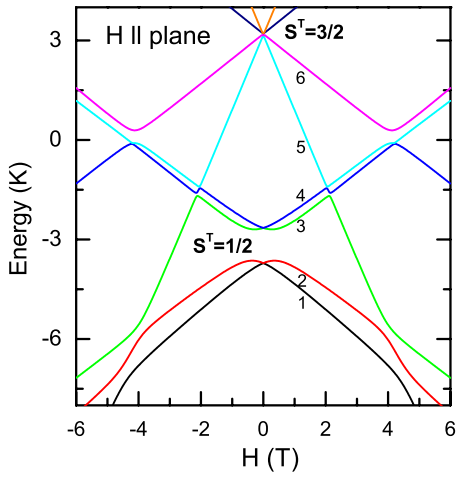

FIG. 8. (Color online) Energy level diagram for {Cu_3-As}. Field dependence of the eight eigenvalues is obtained by solving the Hamiltonian (4) numerically.

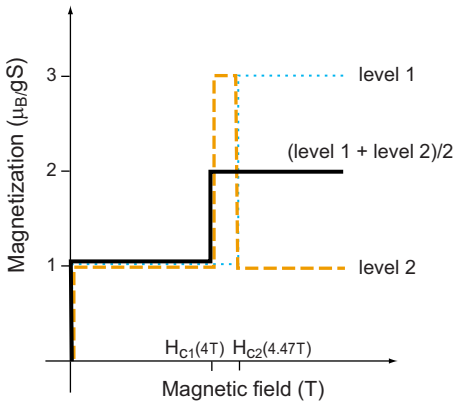

FIG. 9. (Color online) A schematic of magnetization following energy levels 1 and 2 in an upward sweep. See the text for details.

IV. DISCUSSION

To figure out the underlying physics, we first determine the energy level diagram by starting from a general spin Hamiltonian of a spin triangle ring,

$$\mathcal{H} = \sum_{l=1}^{3} \sum_{\alpha=x,y,z} J_{ll+1}^{\alpha} \mathbf{S}_l \cdot \mathbf{S}_{l+1} + \sum_{l=1}^{3} \mathbf{D}_{ll+1} \cdot [\mathbf{S}_l \times \mathbf{S}_{l+1}] + \mu_B \sum_{l=1}^{3} \mathbf{S}_l \cdot \tilde{\mathbf{g}}_{ll} \cdot \mathbf{H}_l, \quad (4)$$

where the exchange coupling constants J_{ll+1}^{α}, the DM vectors $\mathbf{D}_{ll+1}$, and the g-tensors $\tilde{\mathbf{g}}_{ll}$ are defined as site-dependent quantities with a periodic boundary condition.

The magnetic parameters are obtained by diagonalizing the 8×8 matrix numerically. We stress that all parameters are uniquely fixed by considering (i) a crystal symmetry, (ii) the positions of the magnetization steps (see Fig. 2), and (iii) angular dependence of the ESR signals [see Figs. 4(b) and 4(c)]. The resulting values are listed in Table I, and the corresponding energy level diagram is depicted in Fig. 8. Overall, the magnetic parameters of {Cu_3-Sb} are slightly smaller than those of {Cu_3-As}. This is consistent with an increase of Cu···Cu distance upon replacing As with Sb.

TABLE I. A comparison of the magnetic parameters of the {Cu_3-X} compounds.

Magnetic parameters	{Cu_3-As}	{Cu_3-Sb}
$J_{12}^x = J_{12}^y$	4.50 K	4.49 K
J_{12}^z	4.56 K	4.54 K
$J_{23}^x = J_{23}^y = J_{31}^x = J_{31}^y$	4.03 K	3.91 K
$J_{23}^z = J_{31}^z$	4.06 K	3.96 K
$D_{12}^z = D_{23}^z = D_{31}^z$	0.529 K	0.517 K
$D_{12}^x = D_{12}^y$	0.529 K	0.517 K
$g_{11}^{xx} = g_{11}^{yy}$	2.25	2.24
$g_{22}^{xx} = g_{22}^{yy}$	2.10	2.11
$g_{33}^{xx} = g_{33}^{yy}$	2.40	2.40
$g_{ii}^{zz} (i=1-3)$	2.06	2.07

The determined energy levels show that the excited state of $S^T = 3/2$ lies about 6 K above the $S^T = 1/2$ ground state. In addition, the two $S^T = 1/2$ states are split with a sizable energy gap of about 1 K. With the aid of numerical simulations, we find that both the strong DM interactions, amounting to 12% of J_{ij}, and a small isosceles distortion contribute equally to the opening of the gap. This also leads to a lifting of two different spin chiral states, which are defined as

$$\phi_1 = (|\uparrow\downarrow\downarrow\rangle + e^{2\pi i/3}|\downarrow\uparrow\downarrow\rangle + e^{4\pi i/3}|\downarrow\downarrow\uparrow\rangle)/\sqrt{3},$$

$$\phi_2 = (|\uparrow\downarrow\downarrow\rangle + e^{4\pi i/3}|\downarrow\uparrow\downarrow\rangle + e^{2\pi i/3}|\downarrow\downarrow\uparrow\rangle)/\sqrt{3}.$$

On applying an external field, a $S^T = 1/2$ state crosses with a $S^T = 3/2$ state at 2 T and then the ground state changes to a $S^T = 3/2$ state at 4.47 T. We note that the two different spin chiral states show different level crossings with the $S^T = 3/2$ states; energy level 1 has an antilevel crossing with the $S^T = 3/2$ state, while energy level 2 shows a tiny admixture to it in the field interval of 4–4.47 T.

Based on this fact, we can provide an explanation for the observed magnetization features. At 0.4 K, the spins mostly occupy levels 1 and 2 since they are separated by about 1 K from the higher energy levels. When the field is swept upwards, the spins of level 1 transit to the lowest $S^T = 3/2$ state at $H_{C2} = 4.47$ T. The respective magnetization (thin dotted line) is sketched in Fig. 9. The magnetization jump by $1gS\mu_B$ at zero field is attributed to the opening of the tiny gap between the $S^T = 1/2$ states. As possible origins, dipolar interactions and/or intramolecule hyperfine couplings are discussed, but there is yet no consensus on the exact mechanism.[26] The magnetization jump of $2gS\mu_B$ at $H_{C2} = 4.47$ T arises from the level crossing between the $S^T = 1/2$ and $S^T = 3/2$ states. Level 2 undergoes successive transitions of $S^T = 1/2 \rightarrow S^T = 3/2 \rightarrow S^T = 1/2$ (dashed line). Thus, the magnetization by $2gS\mu_B$ will occur in the field regime between H_{C1} and H_{C2}. If we assume that the field sweeping rate is faster than the relaxation rate between levels 1 and 2, the

resulting magnetization will be given by the average of the two processes, yielding the half-step magnetization of $1gS\mu_B$ (see the solid thick line in Fig. 9). The observed step of $1.3gS\mu_B$ is somewhat bigger. A rough estimate suggests that 15% of spins relax from level 2 to level 1 in the course of the field sweeping.

Above 8 T, the magnetization increases continually from $2.3gS\mu_B$ to $3gS\mu_B$. Upon approaching point B of 12 T, the field sweep speed, dH/dt, goes to zero [see a cosine type time evolution of the pulsed field in the middle inset of Fig. 1]. Thus, the spins in level 1 undergo a thermal relaxation to the ground state on approaching 12 T. In the down sweep after the saturation, the spins are confined in level 1. As a result, the magnetization will be governed by level 1: $S^T=3/2 \rightarrow S^T=1/2 \rightarrow S^T=1/2 \rightarrow S^T=3/2$ (thin dotted line). This result suggests that in the *down sweep*, the *thermal relaxations* can be *quenched* and, thus, *spins* can be *decoupled* from environments. This is an important result since the *decoupling leads to enhanced coherence times* for quantum computation. We note that the time interval of the decoupled spin state amounts to several milliseconds (see the inset of Fig. 1). This implies that a dephasing time of the electron spins is estimated to be the same order of magnitude, which is much longer than the switching time of a modern electronic device.

Compared to {Cu_3-As}, the magnetization of {Cu_3-Sb} becomes more symmetric. At the same time, the difference between the up and down sweeps becomes smaller. This implies fast repopulation of the spins between levels 1 and 2. This fact is surprising considering that the spin triangle configuration changes marginally by replacing X. The field dependence of the nuclear spin-lattice relaxation rate $1/T_1$ provides additional insight. At an antilevel crossing point, a strong enhancement of $1/T_1$ is expected due to cross relaxation effects or magnetization fluctuations.[27] For {Cu_3-As}, we find no pronounced peaks around the antilevel crossing points. In contrast, {Cu_3-Sb} shows the peaks at 2 and 4.47 T. Since the magnetic parameters and the energy level structures of the two compounds are nearly the same, the different magnetization and $1/T_1$ behavior indicate that there exists an additional relaxation channel. Since the static lattice structure of {Cu_3-X} hardly depends on X, a lattice vibration might be the responsible factor.[17]

The {Cu_3-X} cluster contains internal vibration modes of the copper triangle subunit. In a regular triangle, a breathing vibration will conserve symmetry. As a result, there will be no mixing between the two $S^T=1/2$ ground states which are orthogonal to each other. However, an out-of-phase stretching vibration will break the local symmetry. Then, the *dynamical* lattice distortion will cause an admixture of the two chiral states 1 and 2, just as the static lattice distortions do. Actually, such a dynamical effect is inferred theoretically in the quantum tunneling of {Fe_{10}} ring.[17] Due to the larger atom size of Sb, the deviation from a regular triangle is slightly bigger in {Cu_3-X}. In this case, we expect more enhanced effect of a dynamical lattice distortion on spin relaxation in {Cu_3-Sb} than in {Cu_3-As}. This explains qualitatively the faster spin relaxation and the more symmetric magnetization observed in {Cu_3-Sb}. We recall that the material dependence of magnetization is also found in the triangles made of V^{4+} ions.[8] Our study indicates that a spin-lattice coupling might be a significant channel of decoherence in the spin triangle.

Finally, we address the potential of a spin triangle as a molecular switch or quantum computation. We start with a triangle with a linear chain consisting of three $S=1/2$ spins. If the system has a sizable uniaxial anisotropy and ferromagnetic exchange coupling, it can be regarded as a SMM, where two $S_z=\pm 3/2$ spin states comprise a memory unit. A quantum spin gate operation may be possible by using pulsed electron paramagnetic resonance technique if the three spins have different g values. In such a scheme, all possible spin states of $S^T=3/2$ are utilized, and thus, it is more effective than other SMMs. However, much work is needed for its realization because of a fast relaxation of $S^T=1/2$ spin.

In the case of AF coupled triangle spin rings, we can adopt a different scheme by exploiting an internal degree of freedom: spin chirality. The right and/or left spin chiralities are well-defined and distinguishable quantum states. Above all, the relaxation time of a chiral state can be as slow as a few milliseconds as shown in the magnetization study of {Cu_3-X}. This is because a spin chirality is defined for the whole triangle and, thus, the fluctuations of individual spin are not crucial. The most remarkable feature is that a tunneling gap, a mixing between two spin chiralities, and a resulting decoherence time can be tuned by controlling molecular symmetry. As shown in Fig. 8, the tunneling gap originates from the DM interaction, which is closely related to a structural chirality. Further, the present NMR study uncovers that the mixing between the two chiral states is determined by the structural distortion from a regular triangle, that is, deviation from C_3 symmetry. Thus, we see that there are two control knobs of a quantum state in a spin triangle: (i) a structural chirality and (ii) a structural distortion. If we attach a photoreactive molecule to the triangle, an induced structural change might control the tunneling gap. This also indicates that an excitation of resonant phonons pertaining to dynamical distortion modes might be possible.

Next we discuss other sources of decoherence: dipolar interaction and nuclear hyperfine interaction. Compared to other SMMs, the dipolar interaction is less serious in a spin triangle because the total spin is as small as $S=3/2$. Such weak interactions can be suppressed by means of a fast sweeping magnetic field as shown in the present work. In this context, an effect of nuclear spins (e.g., hydrogen) on nonmagnetic ions can be quenched as well. In addition, the application of high magnetic field leads to the suppression of the relaxation rate as indicated by the steady decrease of $1/T_1$ with increasing magnetic fields. Regarding the on-site hyperfine coupling, it cannot be avoided by the dilution of material. This problem can be overcome with the help of the chemical engineering of nuclear spins. A considerably long decoherence time is expected for a spin triangle made of nuclear-spin-less $S=1/2$ ions. We note that many well established procedures are currently available for a coherent manipulation of nuclear spin polarization. Thus, it may be possible to manipulate the flip of electron spin via the nuclear spin.[26]

V. CONCLUSIONS

We have presented a comparative study of the $S=1/2$ $\{Cu_3\text{-}X\}$ (X=As and Sb) spin triangle systems using pulsed-field magnetization, Q-band ESR, and ^{23}Na NMR T_1 measurements. The analysis of ESR measurements needed the introduction of the Dzyaloshinskii-Moriya interaction. The hysteresis loops were found to be quite pronounced and indicative of adiabatic quantum tunneling. We find that the magnetization and $1/T_1$ behavior is sensitive to the type of heteroatom X. $1/T_1$ shows a clear peak at the antilevel crossing when X=As, but less so when X=Sb. This is attributed to the different dynamical mixing of a $S=1/2$ chiral state between the two compounds, caused by a coupling of the spins to the lattice vibration. Also, it is seen that a field sweep rate can be adjusted to decouple the spins from the environment. This should lead to enhanced decoherence times, a prerequisite for efficient quantum computation. The present work, thus, indicates that a spin triangle is a promising candidate for molecular implementation of the quantum spin information process. Its extension to $\{Cu_4\}$ and $\{Cu_5\}$ rings[28,29] seems worthwhile.

ACKNOWLEDGMENTS

This work was partly supported by Grant-in-Aid for Scientific Research on priority Areas "High Field Spin Science in 100 T" (No. 451) from MEXT, Japan, NSF Grant No. DMR-0506946, and DFG Grant No. KO-2288/6-1.

[1] D. Gatteschi, R. Sessoli, and J. Villain, *Molecular Nanomagnets* (Oxford University Press, New York, 2006).
[2] D. Gatteschi and R. Sessoli, Angew. Chem., Int. Ed. **42**, 268 (2003).
[3] L. Thomas, F. Lionti, R. Ballou, D. Gatteschi, R. Sessoli, and B. Barbara, Nature (London) **383**, 145 (1996).
[4] W. Wernsdorfer and R. Sessoli, Science **284**, 133 (1999).
[5] E. del Barco, A. D. Kent, S. Hill, J. M. North, N. S. Dalal, E. M. Rumberger, D. N. Hendrickson, N. Chakov, and G. Christou, J. Low Temp. Phys. **140**, 119 (2005).
[6] O. Waldmann, T. Guidi, S. Carretta, C. Mondelli, and A. L. Dearden, Phys. Rev. Lett. **91**, 237202 (2003).
[7] I. Rousochatzakis, Y. Ajiro, H. Mitamura, P. Kögerler, and M. Luban, Phys. Rev. Lett. **94**, 147204 (2005).
[8] T. Yamase, E. Ishikawa, K. Fukaya, H. Nojiri, T. Taniguchi, and T. Atake, Inorg. Chem. **43**, 8150 (2004).
[9] S. Miyashita and N. Nagaosa, Prog. Theor. Phys. **106**, 533 (2001).
[10] M. Luban, F. Borsa, S. Bud'ko, P. Canfield, S. Jun, J. K. Jung, P. Kögerler, D. Mentrup, A. Müller, R. Modler, D. Procissi, B. J. Suh, and M. Torikachvili, Phys. Rev. B **66**, 054407 (2002).
[11] K.-Y. Choi, Y. H. Matsuda, H. Nojiri, U. Kortz, F. Hussain, A. C. Stowe, C. Ramsey, and N. S. Dalal, Phys. Rev. Lett. **96**, 107202 (2006).
[12] D. Gatteschi, L. Pardi, A. L. Barra, A. Müller, and J. Döring, Nature (London) **354**, 463 (1991).
[13] Z. H. Jang, K. H. Han, B. J. Suh, D. Ii, D.-Y. Jung, K.-Y. Choi, and H. Nojiri, J. Korean Phys. Soc. **50**, 464 (2007).
[14] B. Cage, F. A. Cotton, N. S. Dalal, E. A. Hillard, B. Rakvin, and C. M. Ramsey, J. Am. Chem. Soc. **125**, 5270 (2003).
[15] S. Carretta, P. Santini, G. Amoretti, F. Troiani, and M. Affronte, Phys. Rev. B **76**, 024408 (2007).
[16] A. Morello, P. C. E. Stamp, and I. S. Tupitsyn, Phys. Rev. Lett. **97**, 207206 (2006).
[17] H. Nakano and S. Miyashita, J. Phys. Soc. Jpn. **71**, 2580 (2002).
[18] U. Kortz, N. K. Al-Kassem, M. G. Savelieff, N. A. Al Kadi, and M. Sadakane, Inorg. Chem. **40**, 4742 (2001).
[19] A. C. Stowe, S. Nellutla, N. S. Dalal, and U. Kortz, Eur. J. Inorg. Chem. **2004** (19), 3792.
[20] H. Nojiri, R. Taniguchi, Y. Ajiro, A. Müller, and B. Barbara, Physica B **346-347**, 216 (2004).
[21] R. M. Achey, P. L. Kuhns, A. P. Reyes, W. G. Moulton, and N. S. Dalal, Phys. Rev. B **64**, 064420 (2001).
[22] S. H. Baek, M. Luban, A. Lascialfari, E. Micotti, Y. Furukawa, F. Borsa, J. van Slageren, and A. Cornia, Phys. Rev. B **70**, 134434 (2004).
[23] D. Procissi, B. J. Suh, J. K. Jung, P. Kögerler, R. Vincent, and F. Borsa, J. Appl. Phys. **93**, 7810 (2003).
[24] D. Procissi, A. Shastri, I. Rousochatzakis, M. A. Rifai, P. Kögerler, M. Luban, B. J. Suh, and F. Borsa, Phys. Rev. B **69**, 094436 (2004).
[25] M. Affronte, A. Cornia, A. Lascialfari, F. Borsa, D. Gatteschi, J. Hinderer, M. Horvatic, A. G. M. Jansen, and M.-H. Julien, Phys. Rev. Lett. **88**, 167201 (2002).
[26] H. Nojiri, K.-Y. Choi, and N. Kitamura, J. Magn. Magn. Mater. **310**, 1468 (2007).
[27] M. H. Julien, Z. H. Jang, A. Lascialfari, F. Borsa, M. Horvatic, A. Caneschi, and D. Gatteschi, Phys. Rev. Lett. **83**, 227 (1999).
[28] U. Kortz, S. Nellutla, A. C. Stowe, N. S. Dalal, J. van Tol, and B. S. Bassil, Inorg. Chem. **43**, 144 (2004).
[29] S. Nellutla, J. van Tol, N. S. Dalal, L.-H. Bi, U. Kortz, B. Keita, L. Nadjo, G. Khitrov, and A. G. Marshall, Inorg. Chem. **44**, 9795 (2005).